ACS APPLIED MATERIALS & INTERFACES

www.acsami.org

Research Article

Cuboidal Deformation of Multimaterial Composites Prepared by 3-D Printing of Liquid Crystalline Elastomers

Joselle M. McCracken,[‖] Grant E. Bauman,[‖] Graham Williams, Misael Santos, Lawrence Smith, Robert MacCurdy, and Timothy J. White*

Cite This: *ACS Appl. Mater. Interfaces* 2024, 16, 69851−69857

Read Online

ACCESS | Metrics & More | Article Recommendations | Supporting Information

ABSTRACT: Multimaterial 3-D printing (3DP) of isotropic (IsoE) and liquid crystalline elastomers (LCE) yields spatially programmed elements that undergo a cuboidal shape transformation upon heating. The thermomechanical deformation of 3DP elements is determined by the geometry and extent of the isotropic and anisotropic regions. The synthesis and experimental characterization of the 3DP elements are complemented by finite element analysis (FEA). Calculations emphasize that the cuboidal deformation of the myriad 3DP elements is a manifestation of local stress gradients imparted by local control of the material composition and anisotropy. Varying the rectilinear spatial distribution of the multimaterial elastomer composites produces complex, multistable states that provide insights into how stress gradients drive multimaterial elastomer actuation. The thermomechanical stimuli response of the multimaterial elements is explored as a tactile element.

KEYWORDS: *liquid crystalline elastomer, 3-D printing, direct ink writing, multimaterial, actuator, finite element analysis, haptics*

INTRODUCTION

Liquid crystalline elastomers (LCEs) have long been considered as material actuators due to their inherent stimuli response that originates from the ordering of their liquid crystalline (LC) mesogens.[1,2] The earliest examples of LCE actuators utilized an anisotropic shape change associated with a thermally driven transition from an ordered nematic state to a disordered isotropic state (T_{NI}). In this transition, aligned LCEs undergo macroscopic shape change as their polymer networks contract along the axis of mesogen alignment (e.g., the nematic director, n) and expand orthogonally.[3−5] LCEs in this configuration demonstrate compelling force−displacement outcomes in a multitude of actuating systems such as bilayer hinges for self-propelling soft robots[6] or mechanical switches for temperature-sensitive RFID devices.[7]

To exert force during shape change, material actuators such as LCEs must first deform in response to a stimulus and then resist deformation back to their original shape. Depending on the specific programmed mesogen alignment, this resistance to full flattening in response to load may be a result of bending or stretching deformations. Numerous LCE actuators that rely on bending deformations to exert out-of-plane forces leverage bilayer architectures or gradients of actuation magnitude, yet these systems typically display relatively limited force output.[8−12] Further, bending deformations by definition cannot change the Gauss curvature of a surface unless accompanied by stretching deformations.[13]

Comparatively, LCE actuators that must undergo stretching deformations to return to a flat state exhibit remarkable loadbearing capability. Arrays of such actuators have been shown to lift masses up to 2500× their own upon heating.[14] These LCE actuators are based on theoretical work by Warner and co-workers which predicts that an LCE sheet with a nematic director oriented azimuthally around a central point will transform from flat to cone-shaped upon the nematic−isotropic transition.[15] This orientation of the director emulates a + 1 topological disclination.[16,17] The tip of the actuated cone represents a point of singular Gauss curvature, and therefore, the cone cannot be flattened isometrically (e.g., without stretching deformations). Because stretching deformations are more energetically costly than bending deformations in thin films, this in turn leads to the remarkable loadbearing capability of +1 disclination LCE actuators.[18,19]

To prepare azimuthal +1 disclination LCE actuators, a synthesis technique that is amenable to the spatial patterning of the nematic director must be used.[20] Surface alignment is one established method to create +1 disclination LCE sheets, in which interactions between LCE precursors and command surfaces program the nematic director with microscale resolution.[21] This approach is thickness-limited due to the

Received: August 30, 2024
Revised: November 13, 2024
Accepted: November 18, 2024
Published: December 4, 2024

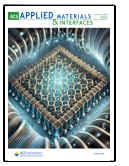

https://doi.org/10.1021/acsami.4c14792
ACS Appl. Mater. Interfaces 2024, 16, 69851−69857

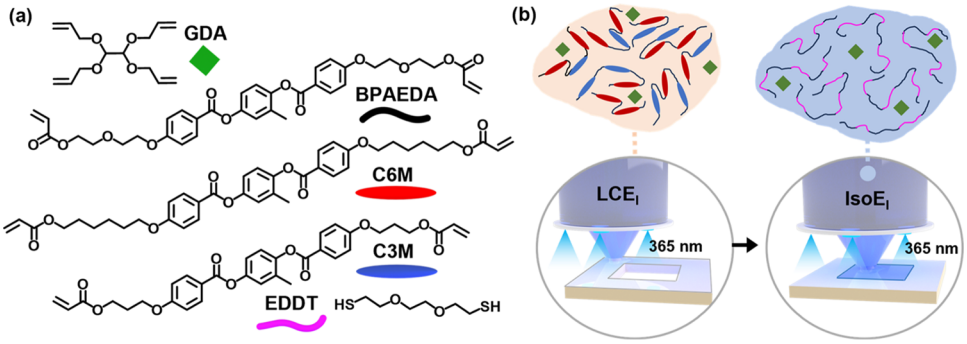

Figure 1. (a) Reagents used in a sequential thiol-Michael/thiol−ene reaction to prepare inks LCE$_I$ and IsoE$_I$ for DIW printing. (b) LCE$_I$ (orange) is an oligomer precursor to the liquid crystalline elastomer and is printed first with low-intensity UV. IsoE$_I$ (blue) is an oligomer precursor to the isotropic elastomer (IsoE) and is printed sequentially then polymerized under high-intensity UV.

short depth through which a command surface induces alignment. For instance, surface-aligned LCEs are limited to thicknesses less than 50 μm unless lamination or direct stacking of LCE films is used to prepare thick, high-force output actuators.[14,22] In the last several years, direct ink write 3-D printing (DIW-3DP) emerged as another widely studied method for spatially patterning LCEs.[23−34] In DIW-3DP of LCEs, viscous inks composed of oligomerized LCE precursors are extruded from a nozzle and subsequently polymerized into solid materials. Shear and extensional forces experienced by LCE inks during extrusion cause the nematic director to align along the print path.[35] This allows for spatial programming of LCEs without the inherent thickness limitations of surface alignment, making this an effective approach to create thick +1 disclination LCE actuators printed in concentric circles or square paths.[23,24,31]

Numerous recent reports describe DIW-3DP cones that result from actuated +1 disclination LCE sheets,[23,31] yet to date, there are few examples of LCEs with complex orientations that produce alternative out-of-plane actuator geometries or are incorporated into multimaterial DIW devices.[36] Recent theoretical work predicts numerous out-of-plane geometric transformations as alternatives to cone geometries that are imminently accessible with multimaterial DIW.[37] These include isotropic elastomer (IsoE) squares, letter shapes, or even feedback interfaces that are driven out-of-plane by an adjacent LCE region for haptics applications.[38−42] These shapes are expected to emerge despite geometric incompatibilities at the active/inactive interfaces.[19] While Gauss curvature at the cone tip is eliminated in these contexts, spatially distinct material properties like those of the IsoE and LCE regions are known to produce new regions of positive and negative Gauss curvature that evolve on either side of interfacial boundaries.[43] Ultimately, flat, elevated surfaces, once experimentally validated, are particularly promising for their greater capability to balance loads, which is not possible without arrays of +1 disclination actuators.

Here, we investigate the thermomechanical properties of one class of these alternative predicted shapes with a series of DIW-3DP cuboidal actuators that develop from heated multimaterial LCE elements. In these, an LCE is printed in azimuthal rectilinear patterns around a central region of an analogous IsoE (e.g., in a concentric square geometry). Upon heating above the T_{NI} of the LCE region, the IsoE region is driven out of plane but itself does not undergo active shape change. Using optical profilometry, we spatially map differences in thermally driven deformation of the multimaterial elastomer elements based on the relative size of the isotropic and anisotropic regions as well as the overall geometry and regions of curvature that emerge at the material interfaces. We find that the multimaterial elements printed with the smallest IsoE regions approximate cone geometries, while the largest IsoE regions produce cuboidal shapes with elevated flat surfaces capable of balancing load.

Finite element analysis (FEA) is used to determine whether the distinct cuboidal shapes resulting from varying spatial composition are a manifestation of local stress gradients. The FEA method is based on an approximation of LCE materials, wherein we ignored the actual mechanism of mesogen alignment and modeled the LCEs as homogeneous materials with an anisotropic coefficient of thermal expansion. Further, we find that conjoining concentric square geometries yield complex, multistable states that provide insights into how stress gradients drive actuation outcomes. Finally, the thermomechanical properties of the cuboidal actuators are explored as insulating tactile feedback elements via thermal imaging, quantitative force measurements, and human touch experiments.

RESULTS AND DISCUSSION

Cuboid Deformation. A series of multimaterial cuboidal actuators are fabricated by DIW-3DP by varying the relative spatial distribution of the LCE and IsoE compositions. The two inks (LCE$_I$ and IsoE$_I$) used to make the multimaterial composite elements are prepared as oligomer/monomer mixtures via a sequential thiol-Michael/thiol−ene chemistry (Figure 1a).[44,45] The principal difference between the LCE$_I$ and IsoE$_I$ compositions is the diacrylate monomer. LCE regions are prepared from the ink LCE$_I$ formulated by mixing two classical LC diacrylate mesogens (C3M, C6M) in a 3:2 mass ratio.[31] IsoE regions are prepared from the ink IsoE$_I$, which is formulated with a non-LC diacrylate monomer (BPAEDA). Blue dye is added to visually distinguish the IsoE region in the multimaterial composite elements. Both ink compositions are melt-mixed and then subjected to base-catalyzed thiol-Michael addition reactions. The inks include a tetrafunctional allyl ether cross-linker (GDA), which does not participate in the thiol-Michael addition reaction. The inks are then extruded via DIW-3DP into a prescribed geometry. Initially, we prepared concentric squares (Figure 1b) of the same overall area with increasing areal density of IsoE (Supporting Information S1). During printing, exposure to low-intensity (2 mW cm^{-2}) 365 nm ultraviolet (UV) light preserves alignment by initiating the thiol−ene reaction of

https://doi.org/10.1021/acsami.4c14792
ACS Appl. Mater. Interfaces 2024, 16, 69851−69857

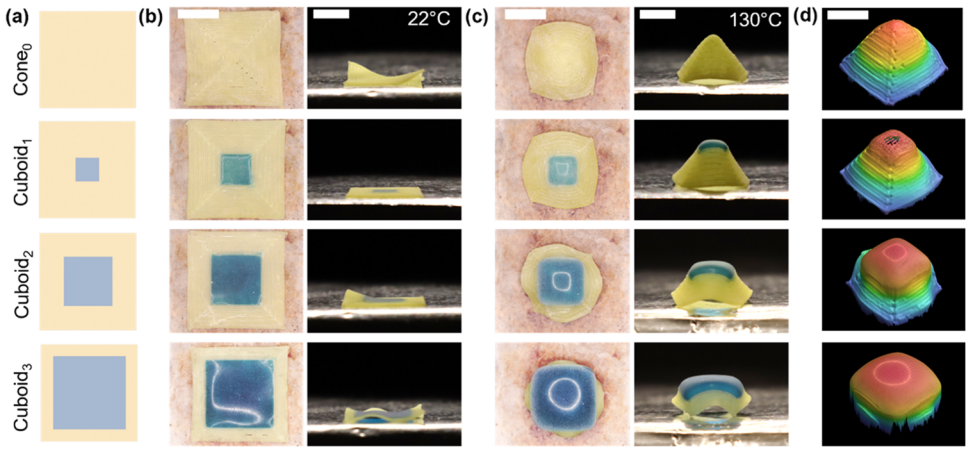

Figure 2. (a) Scheme of LCE (orange) and isoE (blue) spatial distribution in $Cone_0$ and $Cuboid_n$ elements. (b) 2D $Cone_0$ and $Cuboid_n$ elements at 22 °C. (c) Square pyramidal $Cone_0$ and $Cuboid_n$ elements at 130 °C. (d) Profilometric scans of $Cone_0$ and $Cuboid_n$ elements at 130 °C. Scale: 8 mm.

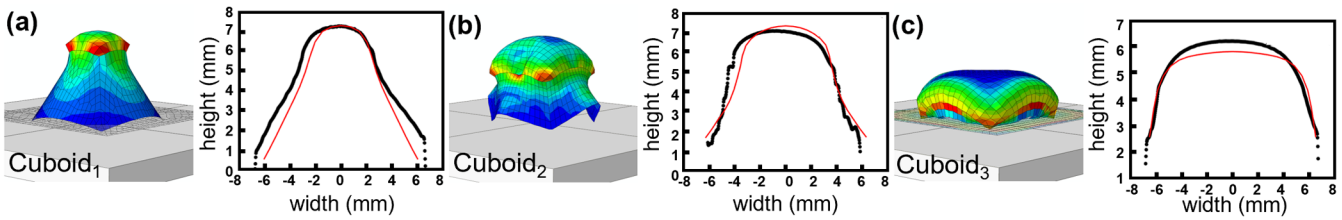

Figure 3. FEA models of (a) $Cuboid_1$, (b) $Cuboid_2$, and (c) $Cuboid_3$ showing greater stress concentrations at the edges and corners of the LCE/IsoE interfaces upon heating. FEA simulated (red) and experimental (black) contours for each $Cuboid_n$ element show good geometric agreement.

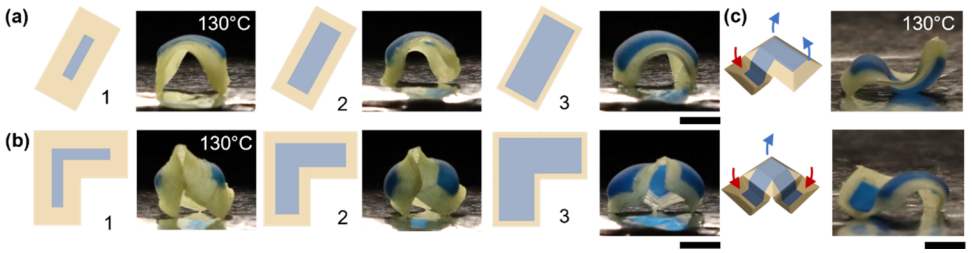

Figure 4. (a) 2:1 Aspect ratio rectangular conjoined $Cuboid_1$, $Cuboid_2$, and $Cuboid_3$ elements with decreasing LCE/IsoE ratios at 130 °C. (b) Right angle conjoined $Cuboid_1$, $Cuboid_2$, and $Cuboid_3$ elements with decreasing LCE/IsoE ratios at 130 °C. (c) Multistable states of $Cuboid_2$ at 130 °C due to eversion of right angle conjoined regions. Scale: 8 mm.

GDA and thiol-capped oligomers. This partial cure step prevents interfacial failures at the boundaries between the inks when they are subsequently cured under high-intensity (50 mW cm^{-2}) 365 nm UV to complete polymerization.

The thermomechanical shape transformations of the multimaterial composites are assessed relative to their proportion of LCE (orange) and IsoE (blue) regions (Figure 2). In contrast, elements prepared entirely from LCE are compared to multimaterial elements with increasing IsoE area (decreasing LCE/IsoE area ratios, Figures 2a and Supporting Information S2). At room temperature (22 °C), both the control and multimaterial elements are predominately flat (Figure 2b). The slight deviation from flatness is associated with shrinkage stress of photopolymerization. Upon heating to 130 °C, the LCE elements form square pyramidal cone shapes (Figure 2c, $Cone_0$) as has been predicted and previously experimentally observed.[15] The multimaterial composites undergo thermomechanical shape transformations to form cuboidal geometries (Figure 2c, $Cuboid_1$, $Cuboid_2$, $Cuboid_3$). The shapes are quantified by profilometric scans (Figure 2d). As is evident in these data, the LCE regions contract azimuthally along the prescribed orientation and expand radially. The unresponsive IsoE regions must accommodate the deformation, which is most accentuated for $Cuboid_3$ as the IsoE area increases (and the LCE/IsoE areal ratio decreases). Further, significant deformation is evident at the boundary between the LCE and the IsoE due to geometric incompatibility. $Cuboid_3$, with the largest boundary and the smallest LCE/IsoE area ratio, exhibits the greatest distortion of the IsoE region.

FEA is utilized to elucidate the stress distribution in the $Cuboid_n$ elements. Simulations produced qualitative stress profiles (Figure 3a–c) which were extracted, and their accuracy is compared to the experimental three-dimensional (3-D) shape characterization (Supporting Information S3). As is evident in Figure 3a–c, the simulation and experiments closely match (confirmed in root-mean-square (rms) error analysis, Supporting Information S4).

https://doi.org/10.1021/acsami.4c14792
ACS Appl. Mater. Interfaces 2024, 16, 69851−69857

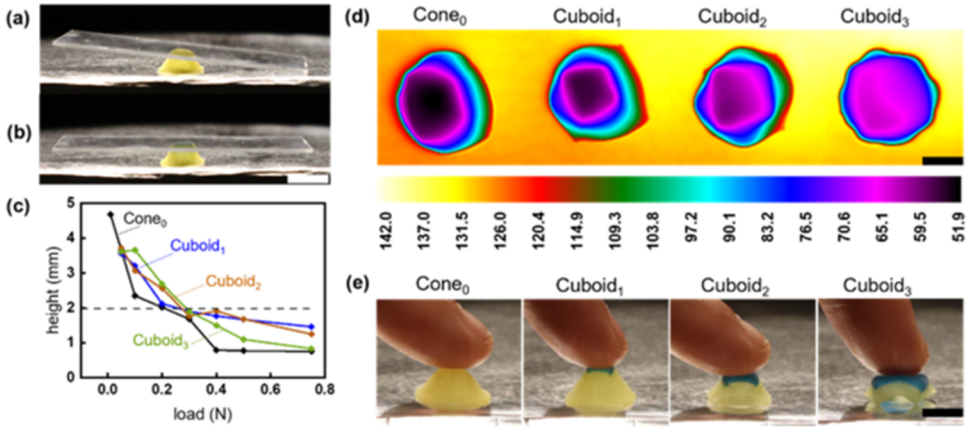

Figure 5. (a) A glass microscope slide on $Cone_0$ does not balance on the element upon heating to 85 °C. Scale 12 mm. (b) A glass microscope slide on $Cuboid_1$ balances on the flat surface of the element. (c) Isostress measurements showing force−displacement profiles for $Cone_0$ and $Cuboid_n$ elements from 0.01 to 0.75 N of load. (d) Infrared images of $Cone_0$ and $Cuboid_n$ elements showing large temperature gradients throughout the actuators on a 130 °C surface. Scale: 8 mm. (e) $Cone_0$ and $Cuboid_n$ elements are safe to the touch on a 130 °C surface. Scale: 12 mm.

Stress Gradients in Conjoined Cuboids. Computational predictions of shape transformation in multimaterial composites suggest that the cuboidal deformation can be spatially programmed.[19] Unfortunately, the experimental manifestation of these predictions deviates due to the stress gradients at the boundaries between IsoE and LCE compositions. To illustrate and isolate this deviation, we used DIW-3DP to conjoin two multimaterial cuboids into rectangles with a 2:1 overall aspect ratio. The conjoined cuboid series consists of LCE perimeters and IsoE interiors prepared with a uniform total area and decreasing LCE/IsoE area ratios (Figure 4a). Upon heating, these multimaterial elements buckle into curved geometries for which the degree of interior curvature is highest when the relative LCE area is greatest (Figure 4a-1). When three cuboids are conjoined at right angles, again with uniform total area and decreasing LCE/IsoE area ratios, the curvature becomes even more complex (Figure 4b) and the elements fold upon themselves. The elements with the highest degree of interior curvature contain the greatest relative LCE area. Generally, it is clear from the comparison of the deformation of square and rectangular cuboids that pattern asymmetry results in geometric incompatibility. As observed previously in arrays of voxelated LCE defects,[46] the conjoined rectangular cuboids can adopt multiple (meta)stable states. This is illustrated in Figure 4c, which shows a right angle conjoined $Cuboid_2$ with one and two regions selectively everted.

Insulated Thermomechanical Actuation and Haptics. Extensive prior examination of LCEs as material actuators has examined the thermomechanical deformation of cones and arrays of cones prepared from spatially patterned LCE elements. While the force output of these low-density soft actuators is compelling, it is often difficult to utilize the shape transformation due to the difficulty in balancing load at the cone apex. This is illustrated in Figure 5a with the deformation of the $Cone_0$ LCE element. Here, the load (e.g., a glass microscope slide) is not balanced and slips during deformation (Figure 5a). One potential advantage of the flattop deformation of cuboidal multimaterial actuators is the capability to better balance load. This is illustrated in Figure 5b, where $Cuboid_1$ actuates and balances the applied load (Figure 5b). $Cuboid_2$ and $Cuboid_3$ also readily balance and lift similar loads when heated to 85 °C (Supporting Information S5).

$Cone_0$ and $Cuboid_n$ geometries each thermally actuate to a particular height, dependent on applied load. This relationship is quantified with isostress force−displacement experiments wherein a set point force is applied and element height is measured with heating to 130 °C. Intersample variability is accounted for with multiple samples of each geometry across a range of force set points from 0.01 to 0.75 N. These data are plotted in full in Supporting Information S6. Maximum measured values for each element are summarized in Figure 5c. We found that all $Cone_0$ and $Cuboid_n$ geometries support a substantial force of at least 0.2 N while maintaining an actuated height of at least 2 mm. LCE $Cone_0$ geometries buckle in a fashion consistent with what has been reported,[18] with the nearly 5 mm tip height buckling subcritically with only 0.05 N applied load. $Cuboid_n$ geometries all perform similarly to one another, with somewhat shorter heights before load is applied relative to the $Cone_0$ geometry, but with consistently improved height retention (1.5−2 mm $Cuboid_n$ vs 1 mm $Cone_0$) at loads as high as 0.4 N. We attribute this outcome in part to the geometric incompatibility at the interface between the LCE and IsoE regions.

The relationship between storage and loss modulus also changes with temperature, impacting the mechanical gradient at the interface between the LCE and IsoE regions. These values were quantified for both materials through oscillation temperature ramp experiments from −50 to 150 °C (Supporting Information S7). Peak tan delta values occur at −4.5 °C for the LCE and −18 °C for the IsoE, corresponding to the glass transition temperature of each material. Above this temperature, the storage and loss moduli for the IsoE are effectively constant (∼0.06 and 0.02 MPa, respectively), and the LCE storage and loss modulus values vary with temperature (0.2−1.7 and 0.7−0.2 MPa, respectively).

The force−displacement characteristics of cuboidal actuators and anisotropic thermal conductivity of LCEs[47] are promising for tactile applications such as haptics.[48,49] Touch of surfaces with temperatures exceeding 43 °C may cause discomfort in these contexts, so the temperature of the actuated cuboid surfaces is characterized by infrared imaging. Because heat is supplied by contact with a heated plate, the actuated elements exhibit large thermal gradients with surface temperatures between 52 and 65 °C when they are heated to 130 °C (Figure 5d). $Cone_0$, with the largest deformation, has

https://doi.org/10.1021/acsami.4c14792
ACS Appl. Mater. Interfaces 2024, 16, 69851−69857

the largest difference in temperature. We attribute the large thermal gradients apparent across all of the cuboidal elements to the low thermal conductivity of elastomers as well as the small contact area with the heated surface. With these surface temperatures, it is feasible to apply haptic pressure for short times (Figure 5e). Supporting Information S8 shows that these elements achieve comparable extent of actuation and force−displacement performance at 85 °C. When heated to 85 °C, the cuboidal elements have surface temperatures that range from 41 and 47 °C, spanning the threshold temperature associated with comfort. This aspect, combined with the force−displacement properties of this series of cuboidal elements, suggests that these materials may serve as haptic surfaces under certain conditions.

CONCLUSIONS

Using multimaterial DIW-3DP, thermotropic LCEs are incorporated into a series of multimaterial cuboid elements capable of lifting flat surfaces out of plane with heating. The geometric incompatibility between the LCE and IsoE regions results in deformation at the edges of the cuboid elements. FEA confirms that stress concentrates at the edges and corners of the LCE/IsoE interface. Complexity of the developed curvature limits the functional design space of these actuators, which is explored by heating conjoined cuboid surfaces (rectangles and right angles). The flat surfaces of the multimaterial cuboid elements naturally balance load better than cones. Further, these elements resist deformation under loads that are on the order of those exerted by human fingers in haptic contexts. Due to the small contact area with the heated surface and the low thermal conductivity of the LCEs, the actuators can be touched even when placed on a 130 °C surface, suggesting applications in haptics or feedback surfaces.

METHODS

Preparation of LCE and Isotropic DIW Inks. Oligomers are prepared through the reaction of a dithiol monomer EDDT (2,2′-(ethylenedioxy) diethanethiol, Aldrich) with diacrylate monomers C6M (1,4-bis-[4-(6-acryloyloxy-hexyloxy)benzoyloxy]-2-methylbenzene, Wilshire Technologies), C3M (1,4-bis(4-[3-acryloyloxybutyloxy]benzoyloxy)-2-methylbenzene, Wilshire Technologies), and BPAEDA (Bisphenol A ethoxylate diacrylate, M_W ∼ 512 g/mol, Aldrich). Included with these monomers are base catalyst DPA (dipropylamine, Aldrich), radical inhibitor BHT (butylated hydroxytoluene, Acros Organics), and photoinitiator I369 (Irgacure 369, IGM Resins). Nonliquid crystalline oligomers are dyed blue by the inclusion of dichroic dye AB4 (Nematel). After DIW-3DP, oligomers are cross-linked by reaction with the four-functional cross-linker GDA (glyoxal bis(diallyl acetal), Aldrich). All reagents are used as received.

Diacrylate monomers, BHT, and I369 are melted and vortex-mixed inside a glass vial using a heat gun at 99 °C. Cross-linker-ene GDA, base catalyst DPA, and dithiol EDDT are added to the vial in order, and the mixture is again vortex-mixed. The molar ratio of acrylate/thiol/ene functional groups is 0.8:1:0.2 for all materials, with masses of components in oligomer synthesis included in Supporting Information S9. Oligomers made with BPAEDA as the diacrylate monomer also contain 0.05 wt % of AB4 added during this step. Following mixing, the vials are sealed and placed on a 65 °C hot plate for 3 h for the thiol-Michael addition reaction to occur. After 3 h, the vials are transferred to an 80 °C oven for 1 h to ensure complete conversion of acrylate groups.

Multimaterial DIW Printing. DIW-3DP is performed with a Hyrel3D System 30 M printer equipped with two KR2 printheads. Prior to printing, oligomers are heated to 65 °C for 5 min and then cooled to ambient temperature. Prints are performed in two layers at a speed of 6 mm s^{-1} with a layer height of 250 μm for the first layer and 200 μm for the second layer. C3M/C6M Ink LCE_I is printed first in printhead 1, followed by printhead 2 filled with the ink $IsoE_I$. LCE_I oligomers made with C3M/C6M are exposed to ∼2 mW cm^{-2} 365 nm UV light during printing to begin polymerization immediately upon deposition. After DIW-3DP, samples are polymerized under 50 mW cm^{-2} 365 nm UV light for 10 min to complete polymerization. Polymerized samples are removed from poly(vinyl alcohol) (PVA)-coated glass slides by heating to 120 °C, at which point the samples actuate and delaminate from the glass. Samples are then coated with a thin layer of corn starch to eliminate residual surface tackiness (this can cause artifacts during thermal actuation) and improve imaging of surface contours with structured light interference.

3-D Imaging of Actuators. Topographic scans of actuators are measured with a Keyence VR-3200 optical profilometer that uses structured light interference to measure surface contours. Samples are placed on a ceramic heater (Thorlabs) and imaged at set increments of voltage supplied to the heater. A thermocouple is used to correlate this voltage to the sample temperature. At each voltage, samples were allowed to equilibrate for 5 min before scanning.

Finite Element Analysis. To predict deformation of the LCE elements, a finite element model is prepared in Abaqus Explicit using deforming shell elements with an anisotropic coefficient of thermal expansion and a linear elastic material assumption. The undeformed part model, shown in Supporting Information S10, consists of two squares, with the inner square representing the IsoE regions and the outer representing the LCE regions. The control sample $Cone_0$ contains no IsoE region. To best match the orientation of the layers laid down by using DIW-3DP, the outer portion is sectioned into four parallelograms. This part model is meshed with S4R shell elements using the advancing front algorithm for quad-dominated mesh types, which begins with seed points on the outer edges of the part. This is used to provide symmetry in meshing the four parallelograms, since the overall geometry is quadrilateral. For each simulated sample, gravity is active and contact modeling with a ground plane supporting the LCE is enabled. A uniform temperature load described by a ramp function from 0 to 130 °C is prescribed, which ties into the structural deformation without bidirectional coupling between deformation and thermal expansion material properties. The ramp is prescribed over an appropriately slow time scale (1 s) to prevent inertial effects from impacting the results. The coefficients of thermal expansion for each sample are taken from experimental results for linear expansion, transformed to account for anisotropic volume expansion, and slightly tuned (by a factor of 0.89) to provide a better simulation to reality match. This factor is constant for all samples, showing that the experimentally derived linear coefficients extend to area effects well. Reported values for these coefficients and the mapping relation are listed in Supporting Information S11.

Thermomechanical Quantification of Cuboidal Elements. Thermomechanical isostress experiments are performed on a TA Instruments RSA-G2 dynamic mechanical analyzer equipped with a 25 mm diameter stainless steel compression clamp. Samples are loaded onto the bottom plate at 20 °C, at which point a fixed downward axial force is applied to the top plate. After allowing temperature to equilibrate for 1 min, the temperature is ramped to 100 °C at a rate of 3 °C min^{-1} and the height of the top plate is measured.

Storage modulus and loss modulus measurements are performed for the IsoE material and parallel to the aligned director of the LCE material on a TA Instruments DMA-850. Measurements are conducted in a two-step process consisting of an isostrain conditioning step to −50 °C followed by an oscillation temperature ramp to 150 °C at a frequency of 1 Hz and a ramp rate of 5 $°C^{-1}$. Aspect ratios are 1:4 with a preload force of 0.02 N applied to maintain tension on the samples.

https://doi.org/10.1021/acsami.4c14792
ACS Appl. Mater. Interfaces 2024, 16, 69851−69857

■ ASSOCIATED CONTENT

Supporting Information

The Supporting Information is available free of charge at https://pubs.acs.org/doi/10.1021/acsami.4c14792.

Masses of reagents used and further FEA modeling results (PDF)

■ AUTHOR INFORMATION

Corresponding Author

Timothy J. White − *Department of Chemical and Biological Engineering, University of Colorado Boulder, Boulder, Colorado 80309, United States; Materials Science and Engineering Program, University of Colorado Boulder, Boulder, Colorado 80309, United States;* orcid.org/0000-0001-8006-7173; Email: timothy.j.white@colorado.edu

Authors

Joselle M. McCracken − *Department of Chemical and Biological Engineering, University of Colorado Boulder, Boulder, Colorado 80309, United States;* orcid.org/0000-0002-0411-3542

Grant E. Bauman − *Department of Chemical and Biological Engineering, University of Colorado Boulder, Boulder, Colorado 80309, United States*

Graham Williams − *Department of Mechanical Engineering, University of Colorado Boulder, Boulder, Colorado 80309, United States*

Misael Santos − *Department of Chemical and Biological Engineering, University of Colorado Boulder, Boulder, Colorado 80309, United States*

Lawrence Smith − *Department of Mechanical Engineering, University of Colorado Boulder, Boulder, Colorado 80309, United States*

Robert MacCurdy − *Department of Mechanical Engineering, University of Colorado Boulder, Boulder, Colorado 80309, United States*

Complete contact information is available at: https://pubs.acs.org/10.1021/acsami.4c14792

Author Contributions

[‖]J.M.M. and G.E.B. contributed equally to this work. J.M.M. and G.E.B. drafted the manuscript. G.E.B. and M.S. performed the majority of experiments. J.M.M. undertook additional experiments and extensive data analysis. G.P.W. conducted the FEA with guidance and contributions from L.S. and R.M. T.J.W. conceived of and led the research effort. The manuscript was written through contributions of all authors. All authors have given approval to the final version of the manuscript.

Notes

The authors declare no competing financial interest.

■ ACKNOWLEDGMENTS

The authors acknowledge financial support through the US Department of Defense National Defense Science and Engineering Graduates Fellowship (GEB) as well as the Charles Stark Draper Scholars Program (GPW).

■ ABBREVIATIONS

LCE - liquid crystal elastomer; DIW - direct ink write; 3DP - 3-D printing

■ REFERENCES

(1) Kularatne, R. S.; Kim, H.; Boothby, J. M.; Ware, T. H. Liquid Crystal Elastomer Actuators: Synthesis, Alignment, and Applications. *J. Polym. Sci., Part B: Polym. Phys.* **2017**, *55* (5), 395−411.

(2) McCracken, J. M.; Donovan, B. R.; White, T. J. Materials as Machines. *Adv. Mater.* **2020**, *32* (20), No. 1906564.

(3) De Gennes, P.-G.; Hébert, M.; Kant, R. Artificial Muscles Based on Nematic Gels. *Macromol. Symp.* **1997**, *113* (1), 39−49.

(4) Wermter, H.; Finkelmann, H. Liquid Crystalline Elastomers as Artificial Muscles. *ePolymers* **2001**, *1*, No. 013.

(5) Li, M.-H.; Keller, P. Artificial Muscles Based on Liquid Crystal Elastomers. *Philos. Trans. R. Soc., A* **2006**, *364* (1847), 2763−2777.

(6) Kotikian, A.; McMahan, C.; Davidson, E. C.; Muhammad, J. M.; Weeks, R. D.; Daraio, C.; Lewis, J. A. Untethered Soft Robotic Matter with Passive Control of Shape Morphing and Propulsion. *Sci. Rob.* **2019**, *4* (33), No. eaax7044.

(7) Shafiq, Y.; Henricks, J.; Ambulo, C. P.; Ware, T. H.; Georgakopoulos, S. V. A Passive RFID Temperature Sensing Antenna With Liquid Crystal Elastomer Switching. *IEEE Access* **2020**, *8*, 24443−24456.

(8) Barnes, M.; Cetinkaya, S.; Ajnsztajn, A.; Verduzco, R. Understanding the Effect of Liquid Crystal Content on the Phase Behavior and Mechanical Properties of Liquid Crystal Elastomers. *Soft Matter* **2022**, *18* (27), 5074−5081.

(9) Yuan, C.; Roach, D. J.; Dunn, C. K.; Mu, Q.; Kuang, X.; Yakacki, C. M.; Wang, T. J.; Yu, K.; Qi, H. J. 3D Printed Reversible Shape Changing Soft Actuators Assisted by Liquid Crystal Elastomers. *Soft Matter* **2017**, *13* (33), 5558−5568.

(10) Kondo, M.; Miyasato, R.; Naka, Y.; Mamiya, J.; Kinoshita, M.; Yu, Y.; Barrett, C. J.; Ikeda, T. Photomechanical Properties of Azobenzene Liquid-Crystalline Elastomers. *Liq. Cryst.* **2009**, *36* (10−11), 1289−1293.

(11) White, T. J.; Serak, S. V.; Tabiryan, N. V.; Vaia, R. A.; Bunning, T. J. Polarization-Controlled, Photodriven Bending in Monodomain Liquid Crystal Elastomer Cantilevers. *J. Mater. Chem.* **2009**, *19* (8), 1080−1085.

(12) Zhang, C.; Lu, X.; Fei, G.; Wang, Z.; Xia, H.; Zhao, Y. 4D Printing of a Liquid Crystal Elastomer with a Controllable Orientation Gradient. *ACS Appl. Mater. Interfaces* **2019**, *11* (47), 44774−44782.

(13) Pressley, A. Gauss' Theorema Egregium. In *Elementary Differential Geometry*, Springer Undergraduate Mathematics Series; Springer: London, 2010; pp 247−268.

(14) Guin, T.; Settle, M. J.; Kowalski, B. A.; Auguste, A. D.; Beblo, R. V.; Reich, G. W.; White, T. J. Layered Liquid Crystal Elastomer Actuators. *Nat. Commun.* **2018**, *9* (1), No. 2531.

(15) Modes, C. D.; Bhattacharya, K.; Warner, M. Gaussian Curvature from Flat Elastica Sheets. *Proc. R. Soc. A* **2011**, *467* (2128), 1121−1140.

(16) McConney, M. E.; Martinez, A.; Tondiglia, V. P.; Lee, K. M.; Langley, D.; Smalyukh, I. I.; White, T. J. Topography from Topology: Photoinduced Surface Features Generated in Liquid Crystal Polymer Networks. *Adv. Mater.* **2013**, *25* (41), 5880−5885.

(17) Kowalski, B. A.; Mostajeran, C.; Godman, N. P.; Warner, M.; White, T. J. Curvature by Design and on Demand in Liquid Crystal Elastomers. *Phys. Rev. E* **2018**, *97* (1), No. 012504.

(18) Duffy, D.; McCracken, J. M.; Hebner, T. S.; White, T. J.; Biggins, J. S. Lifting, Loading, and Buckling in Conical Shells. *Phys. Rev. Lett.* **2023**, *131*, No. 148202.

(19) Davidovitch, B.; Sun, Y.; Grason, G. M. Geometrically Incompatible Confinement of Solids. *Proc. Natl. Acad. Sci. U.S.A.* **2019**, *116* (5), 1483−1488.

(20) Herbert, K. M.; Fowler, H. E.; McCracken, J. M.; Schlafmann, K. R.; Koch, J. A.; White, T. J. Synthesis and Alignment of Liquid Crystalline Elastomers. *Nat. Rev. Mater.* **2022**, *7* (1), 23−38.

(21) de Haan, L. T.; Sánchez-Somolinos, C.; Bastiaansen, C. M. W.; Schenning, A. P. H. J.; Broer, D. J. Engineering of Complex Order and the Macroscopic Deformation of Liquid Crystal Polymer Networks. *Angew. Chem., Int. Ed.* **2012**, *51* (50), 12469−12472.

(22) McCracken, J. M.; Hoang, J. D.; Herman, J. A.; Lynch, K. M.; White, T. J. Millimeter-Thick Liquid Crystalline Elastomer Actuators Prepared by-Surface-Enforced Alignment. *Adv. Mater. Technol.* **2023**, *8* (13), No. 2202067.
(23) Kotikian, A.; Truby, R. L.; Boley, J. W.; White, T. J.; Lewis, J. A. 3D Printing of Liquid Crystal Elastomeric Actuators with Spatially Programed Nematic Order. *Adv. Mater.* **2018**, *30* (10), No. 1706164.
(24) Ambulo, C. P.; Burroughs, J. J.; Boothby, J. M.; Kim, H.; Shankar, M. R.; Ware, T. H. Four-Dimensional Printing of Liquid Crystal Elastomers. *ACS Appl. Mater. Interfaces* **2017**, *9* (42), 37332−37339.
(25) López-Valdeolivas, M.; Liu, D.; Broer, D. J.; Sánchez-Somolinos, C. 4D Printed Actuators with Soft-Robotic Functions. *Macromol. Rapid Commun.* **2018**, *39* (5), No. 1700710.
(26) Davidson, E. C.; Kotikian, A.; Li, S.; Aizenberg, J.; Lewis, J. A. 3D Printable and Reconfigurable Liquid Crystal Elastomers with Light-Induced Shape Memory via Dynamic Bond Exchange. *Adv. Mater.* **2020**, *32* (1), No. 1905682.
(27) Roach, D. J.; Kuang, X.; Yuan, C.; Chen, K.; Qi, H. J. Novel Ink for Ambient Condition Printing of Liquid Crystal Elastomers for 4D Printing. *Smart Mater. Struct.* **2018**, *27* (12), No. 125011.
(28) Ren, L.; Li, B.; He, Y.; Song, Z.; Zhou, X.; Liu, Q.; Ren, L. Programming Shape-Morphing Behavior of Liquid Crystal Elastomers via Parameter-Encoded 4D Printing. *ACS Appl. Mater. Interfaces* **2020**, *12* (13), 15562−15572.
(29) Barnes, M.; Sajadi, S. M.; Parekh, S.; Rahman, M. M.; Ajayan, P. M.; Verduzco, R. Reactive 3D Printing of Shape-Programmable Liquid Crystal Elastomer Actuators. *ACS Appl. Mater. Interfaces* **2020**, *12* (25), 28692−28699.
(30) Wang, Z.; Wang, Z.; Zheng, Y.; He, Q.; Wang, Y.; Cai, S. Three-Dimensional Printing of Functionally Graded Liquid Crystal Elastomer. *Sci. Adv.* **2020**, *6* (39), No. eabc0034.
(31) Saed, M. O.; Ambulo, C. P.; Kim, H.; De, R.; Raval, V.; Searles, K.; Siddiqui, D. A.; Cue, J. M. O.; Stefan, M. C.; Shankar, M. R.; Ware, T. H. Molecularly-Engineered, 4D-Printed Liquid Crystal Elastomer Actuators. *Adv. Funct. Mater.* **2019**, *29* (3), No. 1806412.
(32) Ambulo, C. P.; Ford, M. J.; Searles, K.; Majidi, C.; Ware, T. H. 4D-Printable Liquid Metal−Liquid Crystal Elastomer Composites. *ACS Appl. Mater. Interfaces* **2021**, *13* (11), 12805−12813.
(33) Pozo, M.; Liu, L.; da Cunha, M. P.; Broer, D. J.; Schenning, A. P. H. J. Direct Ink Writing of a Light-Responsive Underwater Liquid Crystal Actuator with Atypical Temperature-Dependent Shape Changes. *Adv. Funct. Mater.* **2020**, *30* (50), No. 2005560.
(34) Ceamanos, L.; Kahveci, Z.; López-Valdeolivas, M.; Liu, D.; Broer, D. J.; Sánchez-Somolinos, C. Four-Dimensional Printed Liquid Crystalline Elastomer Actuators with Fast Photoinduced Mechanical Response toward Light-Driven Robotic Functions. *ACS Appl. Mater. Interfaces* **2020**, *12* (39), 44195−44204.
(35) Bauman, G. E.; Koch, J. A.; White, T. J. Rheology of Liquid Crystalline Oligomers for 3-D Printing of Liquid Crystalline Elastomers. *Soft Matter* **2022**, *18* (16), 3168−3176.
(36) Tabrizi, M.; Clement, J. A.; Babaei, M.; Martinez, A.; Gao, J.; Ware, T. H.; Shankar, M. R. Three-Dimensional Blueprinting of Molecular Patterns in Liquid Crystalline Polymers. *Soft Matter* **2024**, *20* (3), 511−522.
(37) Bouck, L.; Nochetto, R. H.; Yang, S. Reduced membrane model for liquid crystal polymer networks: Asymptotics and computation. *J. Mech. Phys. Sol.* **2024**, *187*, No. 105607.
(38) Torras, N.; Zinoviev, K. E.; Esteve, J.; Sánchez-Ferrer, A. Liquid-Crystalline Elastomer Micropillar Array for Haptic Actuation. *J. Mater. Chem. C* **2013**, *1* (34), 5183−5190.
(39) Bai, H.; Li, S.; Shepherd, R. F. Elastomeric Haptic Devices for Virtual and Augmented Reality. *Adv. Funct. Mater.* **2021**, *31* (39), No. 2009364.
(40) Gao, J.; He, Y.; Cong, X.; Yi, H.; Guo, J. Reconfigurable Fluorescent Liquid Crystal Elastomers for Integrated Visual and Haptic Information Storage. *ACS Appl. Mater. Interfaces* **2022**, *14* (47), 53348−53358.
(41) Fowler, H. E.; Rothemund, P.; Keplinger, C.; White, T. J. Liquid Crystal Elastomers with Enhanced Directional Actuation to Electric Fields. *Adv. Mater.* **2021**, *33* (43), No. 2103806.
(42) Gablier, A.; Terentjev, E. M. Flexible Force-bearing Liquid Crystalline Elastomer Component toward a Dynamic Braille Platform. *Nano. Sel.* **2023**, *4* (5), 324−332.
(43) Kuenstler, A. S.; Chen, Y.; Bui, P.; Kim, H.; DeSimone, A.; Jin, L.; Hayward, R. C. Blueprinting Photothermal Shape-Morphing of Liquid Crystal Elastomers. *Adv. Mater.* **2020**, *32* (17), No. 2000609.
(44) Bauman, G. E.; Koch, J. A.; White, T. J. Rheology of Liquid Crystalline Oligomers for 3-D Printing of Liquid Crystalline Elastomers. *Soft Matter* **2022**, *18* (16), 3168−3176.
(45) Bauman, G. E.; McCracken, J. M.; White, T. J. Actuation of Liquid Crystalline Elastomers at or Below Ambient Temperature. *Angew. Chem., Int. Ed.* **2022**, *61* (28), No. e202202577.
(46) Plucinsky, P.; Kowalski, B. A.; White, T. J.; Bhattacharya, K. Patterning Nonisometric Origami in Nematic Elastomer Sheets. *Soft Matter* **2018**, *14* (16), 3127−3134.
(47) Cang, Y.; Liu, J.; Ryu, M.; Graczykowski, B.; Morikawa, J.; Yang, S.; Fytas, G. On the Origin of Elasticity and Heat Conduction Anisotropy of Liquid Crystal Elastomers at Gigahertz Frequencies. *Nat. Commun.* **2022**, *13*, No. 5248.
(48) Huang, Y.; Zhou, J.; Ke, P.; Guo, X.; Yiu, C. K.; Yao, K.; Cai, S.; Li, D.; Zhou, Y.; Li, J.; Wong, T. H.; Liu, Y.; Li, L.; Gao, Y.; Huang, X.; Li, H.; Li, J.; Zhang, B.; Chen, Z.; Zheng, H.; Yang, X.; Gao, H.; Zhao, Z.; Guo, X.; Song, E.; Wu, H.; Wang, Z.; Xie, Z.; Zhu, K.; Yu, X. A Skin-Integrated Multimodal Haptic Interface for Immersive Tactile Feedback. *Nat. Electron.* **2023**, *6* (12), 1020−1031.
(49) Hong, S.; Gu, Y.; Seo, J. K.; Wang, J.; Liu, P.; Meng, Y. S.; Xu, S.; Chen, R. Wearable thermoelectrics for personalized thermoregulation. *Sci. Adv.* **2019**, *5* (5), No. eaaw0536.

https://doi.org/10.1021/acsami.4c14792
ACS Appl. Mater. Interfaces 2024, 16, 69851−69857